Mass and charge distributions of Cl-induced heavy-ion reactions

A. A. Marchetti,* A. C. Mignerey, H. Madani, A. Gökmen, W.L. Kehoe,†
B. Libby, and K. Morley‡
Department of Chemistry, University of Maryland, College Park, Maryland 20742

H. Breuer
Department of Physics, University of Maryland, College Park, Maryland 20742

K. Wolf§
Argonne National Laboratory, Argonne, Illinois 60439

F. Obenshain
Oak Ridge National Laboratory, Oak Ridge, Tennessee 37831
(Received 19 May 1992)

Projectilelike fragments were detected and characterized in terms of A, Z, and energy for the reactions ^{37}Cl on ^{40}Ca and ^{209}Bi at $E = 7.3$ MeV/nucleon, and ^{35}Cl on ^{209}Bi at $E = 15$ MeV/nucleon, at angles close to the grazing angle. Mass and charge distributions were generated in the N-Z plane as a function of energy loss, and parametrized in terms of their centroids, variances, and coefficients of correlation. The results are compared to the predictions of two current models based on a stochastic nucleon exchange mechanism. The drifts of the charge and mass centroids for the system ^{37}Cl on ^{40}Ca are consistent with a process of mass and charge equilibration mediated by nucleon exchange between the two partners, followed by evaporation. The asymmetric systems show a strong drift toward larger asymmetry, with the production of neutron-rich nuclei. It is concluded that this is the result of a net transfer of protons from the light to the heavy partner, and a net flow of neutrons in the opposite direction. Model predictions fail to reproduce in detail the evolution of the centroids for asymmetric systems. The variances for all systems increase with energy loss, as would be expected from a nucleon exchange mechanism. However, the variances for the reaction ^{37}Cl on ^{40}Ca are higher than those expected from that mechanism, and the variances for the reaction ^{35}Cl on ^{209}Bi start decreasing after about 100 MeV of energy loss. The coefficients of correlation indicate that the transfer of nucleons between projectile and target is correlated, as expected from Q-value constraints to the valley of β stability.

PACS number(s): 25.70.Lm

I. INTRODUCTION

Deep-inelastic heavy-ion reactions at energies close to the Coulomb barrier produce a wide variety of nuclides over kinetic energy losses that can range from tens to hundreds of MeV [1]. Even though there have been numerous studies of these reactions, there are still several aspects that need to be addressed to achieve a better understanding of the deep-inelastic mechanism. Among some of the current questions regarding these reactions are the excitation energy division between projectilelike and targetlike fragments and the drifts of the product distributions in the mass-charge plane. Presently, it is accepted that the exchange of nucleons between projectile and target is largely responsible for the transformation of the incident relative kinetic energy and angular momentum into excitation energy and intrinsic spin of the products. However, coherent modes for energy damping have also been suggested [2]. The drifts in the average neutron number ($\langle N \rangle$) and proton number ($\langle Z \rangle$) of the projectilelike and targetlike fragments are strongly influenced by the driving forces created by the underlying dinuclear potential. On the other hand, the variances of the N and Z distributions are more sensitive to the details of the mechanisms involved. Hence, the study of the product distributions provides the opportunity to study these important aspects of the deep-inelastic mechanism.

Different authors have determined mass and charge distributions of the products of deep-inelastic reactions as a function of total kinetic-energy loss ($E_{\rm loss}$) for a variety of systems, and have characterized the distributions

*Present address: Lawrence Livermore National Laboratory, Livermore, California 94550.
†Present address: Massachusetts Institute of Technology, Cambridge, Massachusetts 02139.
‡Present address: Indiana University Cyclotron Facility, University of Indiana, Bloomington, Indiana 47405.
§Present address: Cyclotron Institute, Texas A&M University, College Station, Texas 77483.

in terms of the different moments in the plane determined by N (or the mass number A) and Z. In several asymmetric projectile-target systems [3–12] it has been found that the charge centroid of the projectilelike fragments shows a drift towards larger asymmetry (negative drift). In all of these cases the projectile has a lower neutron-to-proton (N/Z) ratio than the target, and an increase is observed in the average neutron-to-proton ($\langle N\rangle/\langle Z\rangle$) ratio of the projectilelike fragments. On the other hand, observations made on the system ^{136}Xe on ^{56}Fe, where the projectile has a higher N/Z ratio than the target, showed that the $\langle Z\rangle$ of the projectilelike fragments increased, while the $\langle N\rangle$ decreased [13].

Overall, the experimental evidence indicates that the isospin coordinate equilibrates fast even at the expense of larger mass asymmetry. In principle, the drifts of charge and mass in the N-Z plane should reflect more or less the direction and magnitude of the gradient of the potential-energy surface (PES). The effect of the N/Z ratio on the charge and mass drifts was studied by de Souza *et al.* [14]. For a given target (^{238}U) and for the same bombarding energy per nucleon (E = 8.5 MeV/nucleon), the charge drift was found to be strongly correlated with the N/Z ratio of the projectile and the magnitude of the gradient. No such rigorous correlation was found for the case of the neutron drift, but $\langle N\rangle$ is more susceptible to evaporation effects than $\langle Z\rangle$ in the systems studied by de Souza. For four different systems, Planeta *et al.* [9] depicted the evolution of $\langle N\rangle$ and $\langle Z\rangle$ with $E_{\rm loss}$ in the N-Z plane along with a calculated gradient vector at the injection point. For the system ^{58}Ni on ^{238}U that has the largest gradient, the evolution of the centroids follow very closely the gradient vector. However, for the system ^{74}Ge on ^{165}Ho, the evolution of the centroids departs dramatically from the direction of the calculated gradient.

Some systems [7–9,11,12,15,16] have been compared to predictions of a nucleon exchange transport model that was developed by Randrup [17]. In general, variance predictions are in good agreement with the experimental results. However, the N and Z centroids predicted for asymmetric projectile-target systems have shown significant departures from the experimental centroids. Contrary to the experimental results, the model normally predicts an evolution towards symmetry of the mass coordinate. Another model, also based on nucleon exchange, has been recently developed by Tassan-Got [18]. It has been claimed [19] that predictions from this model are in better agreement with experimental centroids in asymmetric systems. Since both models have much of the same physical foundations, it is interesting to investigate the reasons for such different predictions in the evolution of the centroids.

In this study, the secondary mass and charge distributions of the projectilelike fragments were measured for the systems ^{37}Cl on ^{40}Ca and ^{209}Bi at E = 7.3 MeV/nucleon, and ^{35}Cl on ^{209}Bi at E = 15 MeV/nucleon. The relatively high bombarding energy of the last system should provide a wide energy loss range for the deep-inelastic component of the reaction mechanism and, therefore, for the study of the parameters of interest. However, as energy loss increases, the effects of evaporation become also increasingly important and should be taken into consideration when interpreting the data. The lower-energy systems, besides adding to the systematics, presented the possibility of a comparative study of the effects of N/Z and mass asymmetry on the parameters of the distributions. The parameters of the experimental distributions are compared to those calculated using the two nucleon exchange models already mentioned. Since the models predict only primary distributions, comparisons between model and experiment require corrections to account for evaporation. Either the experimental primary distributions have to be reconstructed from the secondary distributions or the primary distributions from the model have to be subjected to an evaporation calculation to infer the model secondary distributions. In the present study the latter is achieved by feeding the primary distributions predicted by models into the evaporation code PACE II [20] to obtain the secondary distributions, which then are compared with the experimental results.

II. EXPERIMENTAL PART

Two separate experiments were performed. The first one investigated the systems ^{37}Cl on ^{209}Bi and ^{37}Cl on ^{40}Ca at E= 7.3 MeV/nucleon and took place at Argonne National Laboratory. The second studied the system ^{35}Cl on ^{209}Bi at E= 15 MeV/nucleon and took place at the Holifield Heavy Ion Research Facility of Oak Ridge National Laboratory. In both experiments, the time-of-flight (TOF) technique was used to identify the mass number of projectilelike fragments. The atomic number was deduced using the dE-E technique. The off-line data analysis was done using the program LISA [21].

A. ^{37}Cl on ^{40}Ca and ^{209}Bi at E = 7.3 MeV/nucleon

A beam of ^{37}Cl at 270.0 MeV was provided by Argonne's Superconducting LINAC (presently ATLAS). The beam current was maintained between 13 and 50 nA during the experiment. The targets were self-supporting ^{209}Bi and ^{40}Ca and had thicknesses of 700 and 300 μg/cm^2, respectively. The projectilelike reaction products were detected in a silicon detector telescope consisting of a transmission detector with an active area of 50 mm^2 and a thickness of 17.1 μm, and a stop detector with an active area of 300 mm^2. The time of flight was measured between the dE transmission and the E stop detectors. The distance between the transmission and stop detectors was about 62 cm, and the distance between the target and the transmission detector was about 14 cm. Data were collected near the grazing angle: at 13.0° for the Ca target and at 44.0° for the Bi target. The timing resolution achieved was < 100 ps (full width at half maximum, FWHM) and was sufficient to identify all masses of interest. The event trigger was a coincidence between the dE and E detectors.

Nonlinearities in the response of the electronics were checked using a precision calibration pulser and corrected with a second degree polynomial. The energy signal of

each silicon detector was calibrated using a ^{252}Cf fission source. The calibrated energy signals of the dE and E detectors were then added to give the total detected energy, which, in addition, was corrected for pulse-height defects [22]. A final calibration factor (very close to 1.0) positioned the elastic peak exactly at the theoretical elastic energy, minus the calculated energy loss in half of the target thickness. In the later analysis, the tabulated energy and charge-dependent energy loss in half of the target thickness was added to the total detected energy to obtain the actual kinetic energy of the projectilelike fragments. From calibration runs with the Ca target at 8.0°, the energy resolution (FWHM) was 1.7 MeV for the ^{37}Cl elastic peak (265.2 MeV).

The charge and mass calibrations were done using the Ca data at 13.0° because this provided a wider range of charges and masses in the products than did the Bi target. The Z lines and the mass lines were corrected empirically for energy dependence. The correction was considered suitable when the position of the mass or charge centroids did not change by more than 0.1 mass unit when plotted as a function of laboratory energy. It was found that the centroid position of a given mass shifts with the atomic number and vice versa. A linear correction to both the atomic number and the mass was made to eliminate these shifts. The resolutions (FWHM) were 0.5 mass unit for $A = 37$ and 0.4 charge unit for $Z = 17$. Representative charge and mass distributions are shown in Fig. 1.

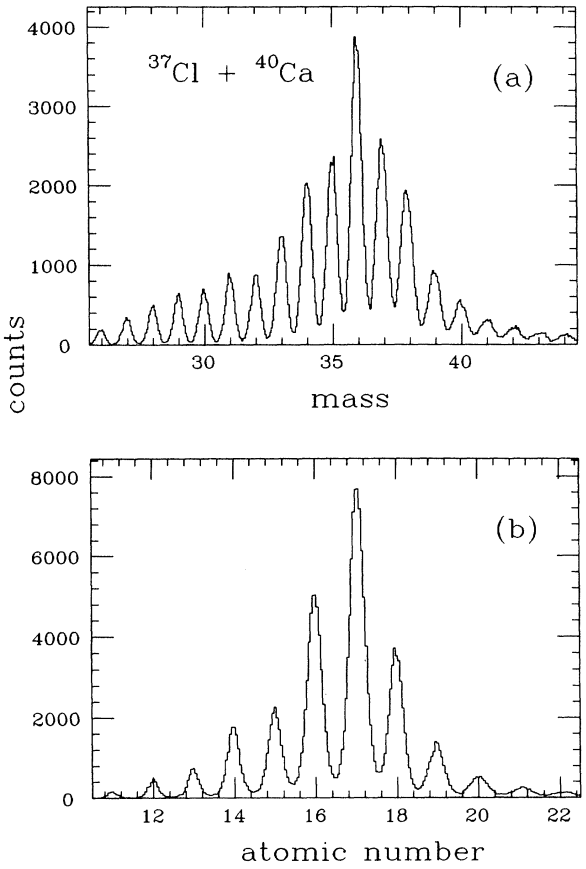

FIG. 1. Representative (a) mass and (b) charge distributions for the system ^{37}Cl + ^{40}Ca at 270 MeV. An energy gate was set to eliminate elastic events.

B. ^{35}Cl on ^{209}Bi at E = 15 MeV/nucleon

A 528.8-MeV beam of ^{35}Cl, provided by the coupled operation of the HHIRF tandem and cyclotron, was delivered to the TOF station. The TOF spectrometer consisted of a 30.5-cm-diam scattering chamber connected to a TOF arm with a dE-E ionization chamber at its end. The beam charge current was maintained between 15 and 20 nA throughout the experiment. The charge state of ^{35}Cl was 14^+; the time structure of the beam was determined by the cyclotron frequency (10.71 MHz.). The target was self-supporting ^{209}Bi (1000 μg/cm^2). A potential of 1500 V was applied to the target to suppress secondary electrons. The TOF arm was positioned at 18.0° for data collection. A collimator consisting of a stainless steel plug with an oval orifice of about 3×6 mm^2 was placed at the entrance of the arm, which was at 15.3 cm from the target. Therefore, the TOF arm provided an angular acceptance of about 0.6° in plane and 1.2° out of plane.

The start and stop detectors used in the TOF measurement were transmission-type parallel plate avalanche counters (PPAC's). They were mounted in the TOF arm separated by a distance of 253 cm. The start detector was positioned at 39.4 cm from the target. The start PPAC had an area of 2×2 cm^2, and the stop PPAC had an area of 8×10 cm^2 and could be enabled to give x-y position information. Each PPAC had four windows made of 60 μg/cm^2 polypropylene. Both detectors were filled with isobutane at a pressure of 6 torr. The ionization chamber at the end of the TOF arm had four consecutive anodes of 10, 10, 20, and 40 cm in length, respectively. The entrance to the chamber was a 300 μg/cm^2 Mylar window. A mixture of 90% Ar and 10% methane (P-10) was used as the filling gas at a pressure of about 410 torr.

Corrections for electronics nonlinearities were performed for each of the four energy signals of the ionization chamber. A partial position correction was applied using the x-position information provided by the measurement of the electron-drift time in the ionization chamber. The x-position dependence of the energy and TOF signals was corrected using polynomials. A gate on this drift-time was also established to reject events either without drift time or near the extremes of the drift-time spectrum of the ionization chamber. After x-position correction, the four dE signals were added together to generate a new parameter proportional to the total-energy deposited in the ion chamber. The addition of the four signals was multiplied by a factor to normalize the total energy to that of the elastic peak minus the energy loss in half of the target thickness and the windows of the detectors.

Corrections for energy loss in half of the target thickness and the windows of the detectors, as a function of atomic number and energy of the projectilelike fragment, were performed in the way described for the Argonne ex-

periment. For the elastic peak at 18.0°, the energy was 520.2 MeV with a FWHM of about 10 MeV. It should be stressed that this width actually represents an upper limit for the energy resolution because the elastic peak was measured close to the grazing angle, where inelastic events contribute significantly to the total width. For the atomic number determination, the first element of the ionization chamber was not used because of its poor resolution. The Z lines were obtained using the second element as the dE parameter and the addition of the third and fourth as the E parameter. As a consequence, events that deposited all their energy in the first two elements did not have Z identification and were not considered. For example, using energy loss calculations, the minimum energies required for the identification of Z= 17, 15, 13, and 11 are about 240, 205, 170, and 135 MeV, respectively. A FWHM of about 0.3 charge unit was measured for $Z = 17$.

The determination of the mass presented a very difficult problem due to the poor resolution obtained for the experimental mass parameter. After establishing a gate around $Z = 17$, the width (FWHM) of the elastic TOF peak measured at 18.0° was about 900 ps. Considering the energy resolution to be around 1% (a value consistent with previous experiments), the resulting mass resolution would have an upper limit of about 1.7 mass units. Without defined peaks, mass cannot be unambiguously corrected for energy dependence because the positions of the centroids cannot be established with certainty. Several attempts to try to elucidate the mass centroids failed. A new approach was tried: the use of deconvolution techniques, commonly used in image restoration, to enhance the mass peaks. The method was successfully tested in known spectra that had been purposely distorted and subsequently applied to the Oak Ridge mass data [23].

To determine the energy dependence of the mass parameter, the yield in the mass-energy plane was obtained for Z= 15, 16, and 17, respectively, and projections of the yield on the mass coordinate were made at 10-MeV energy intervals. The position of the mass peaks corresponding to each projection was established using the deconvolution technique. The energy dependence was corrected for each Z separately. Mass parameters corresponding to $Z < 15$ or $Z > 17$ were corrected assuming the same functional dependence as that of Z=15 or 17, respectively. Mass spectra were then generated individually for $Z = 13$ to 18. The positions of the mass peaks were determined using the deconvolution technique, and the mass parameter was linearly calibrated for Z dependence. After the mass parameter was corrected for energy and Z dependence, a total mass spectrum (excluding only Z=17) was generated and deconvolved. The peak centroids were found at the expected values of the mass coordinate. Mass spectra were also generated and deconvolved for individual atomic numbers after the energy and Z dependence were corrected, and the centroids were found consistent with the mass coordinate. It is important to note that the deconvolution procedure was used with the sole purpose of calibrating the mass parameter, and that it was not applied to any of the spectra used thereafter. In principle, this procedure could only introduce errors to the mass calibration. However, the technique applied to corrected spectra has shown consistency in revealing the mass peaks at the expected positions. Representative mass and charge distributions are shown in Fig. 2; the mass spectrum shows both the original data and the result of applying the deconvolution procedure.

C. Data reduction

The procedures employed for data reduction are similar to those described and used in Refs. [5,8,9,24]. The total kinetic energy loss, $E_{\rm loss}$, was calculated assuming two-body kinematics. Corrections in the energy-loss scale for evaporation were included. The assumptions made in this correction were (1) that the velocity of the projectilelike fragment did not change, on the average, because of evaporation, (2) that the evaporated mass could be expressed as a smooth function of the excitation energy of the projectilelike fragment, and (3) that the ground-state Q value could be expressed as a smooth function of the projectilelike fragment Z. The corrections also need

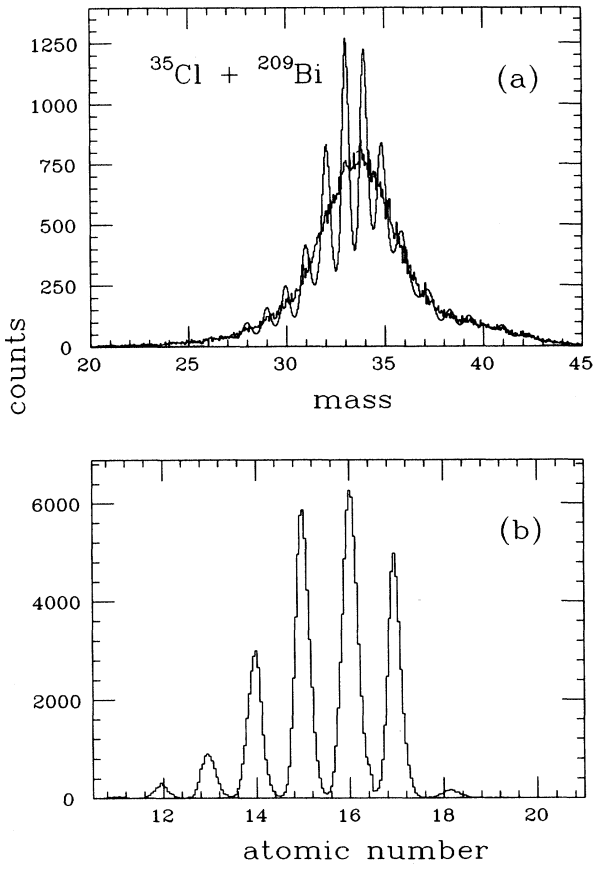

FIG. 2. Representative (a) mass and (b) charge distributions for the system ^{35}Cl + ^{209}Bi at 528 MeV. A gate was set to eliminate elastic events. There are two curves for the mass: one represents the data as is (single wide peak), and the other the peak enhancement effect after using a deconvolution procedure.

to assume a form of excitation energy division between projectilelike and targetlike fragments.

Experimental evidence indicates that the excitation energy divides equally at low-energy losses and smoothly evolves towards thermal equilibrium as the energy loss increases [3,25]. Therefore, two cases were considered for the correction of the energy-loss scale in the case of the Bi reactions: equal division of excitation energy between the reaction partners and division according to the mass of the products (thermal division). Only equal division was considered for the Ca target, since both projectile and target are practically identical in mass.

The total evaporated mass was calculated as a function of excitation energy using the PACE II code [20] for a series of possible reaction products of the systems under study. It was assumed that the reaction products would have N/Z ratios between that of the projectile and that of the composite system. Linear fits were performed to obtain an expression for the average mass evaporated (ΔM) as a function of the excitation energy ($E_{\rm ex}$)

$$\Delta M = m_0 + m_1 E_{\rm ex}, \tag{1}$$

where m_0 and m_1 are constant coefficients. The spin of the particle, one of the inputs to PACE II [20], was calculated assuming the sticking limit [3]. Calculations at fixed spin values ($1\hbar$ and $15\hbar$) showed that the average evaporated mass did not have a strong dependence on the spin. However, the evaporated mass shows greater dispersion for the higher spin, as seen in Fig. 3. Ground state Q values (Q_{gg}) were plotted as a function of the atomic number for each of the systems and fit with a quadratic polynomial:

$$Q_{gg} = q_0 + q_1 Z + q_2 Z^2, \tag{2}$$

where q_0, q_1, and q_2 represent constant coefficients.

The values of the constant coefficients of Eqs. (1) and (2) for each of the three systems studied here are given in Table I. For each event, the step-by-step procedure can be summarized as follows (the numbers 1–4 represent the projectile, target, projectilelike fragment, and targetlike fragment, respectively): (1) Calculate a first estimate of $E_{\rm loss}$ using the experimental $M3$ and $E3$, assuming $M4 = M1 + M2 - M3$. (2) Using Eq. (2), calculate the ground-state Q-value corresponding to the projectilelike fragment Z. (3) Determine the total excitation energy as $E_{\rm loss} - Q_{gg}$. (4) Assume a form of excitation energy division and calculate the excitation energy of the projectilelike fragment. (5) From Eq. (1), calculate the mass evaporated using the excitation energy obtained in step 4, add it to $M3$ and recalculate $M4$. (6) Calculate the energy of the projectilelike fragment by multiplying the original energy by the ratio $(M3 + \Delta M)/M3$. (7) Recalculate $E_{\rm loss}$ and find the difference from the last value obtained. Repeat steps 3–7 until the difference becomes smaller than 0.1 MeV or the number of iterations reaches 100 (abort event). Practically no events were discarded and the latter condition was set only to avoid an infinite loop in case of a bad event.

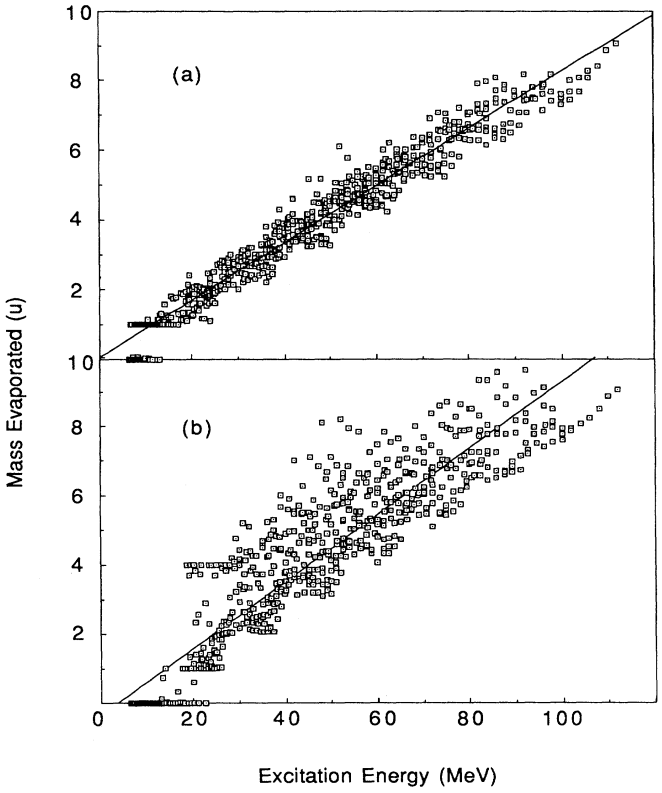

FIG. 3. Mass evaporated as a function of the excitation energy for several possible projectilelike fragments of the reaction ^{35}Cl + ^{209}Bi assuming two different spin values: (a) $1\hbar$ and (b) $15\hbar$. The straight lines are least-square fits to the simulations.

Distributions of atomic and neutron number as a function of $E_{\rm loss}$ were generated. The $E_{\rm loss}$ was binned in 4-MeV intervals for the systems ^{37}Cl on ^{40}Ca and ^{209}Bi, and in 10-MeV intervals for the system ^{35}Cl on ^{209}Bi for the first 100 MeV of $E_{\rm loss}$ and 20-MeV intervals from there on. The wider energy intervals used in the last

TABLE I. Values of the fit parameters corresponding to Eqs. (1) and (2) for the three systems under study.

System	m_0 (10^{-2} u)	$10^2 m_1$ (10^{-2} u/MeV)	q_0 (MeV)	q_1 (MeV/Z)	q_2 (10^{-2} MeV/Z^2)
^{37}Cl on ^{40}Ca	−28.77	9.990	−22.71	2.378	−6.528
^{37}Cl on ^{209}Bi	5.749	8.187	−207.0	16.63	−26.49
^{35}Cl on ^{209}Bi	5.749	8.187	−187.3	15.07	−22.89

system are due to the larger energy-loss range and the poor statistics at high-energy loss. The relative yield of projectilelike fragments was plotted in the N-Z plane, which was binned in cells of 0.25×0.25 mass-charge unit. All the relative yields were transformed to the center-of-mass system and the distributions characterized by their centroids, variances, and coefficients of correlation. Two methods were employed to parametrize the shapes of the distributions: moment analysis and two-dimensional Gaussian fit [24]. Both methods include corrections for finite resolution and binning effects. For the most part, no significant differences were found between the results of the two methods [23]. But, at low $E_{\rm loss}$ values, some significant differences were found. However, in this energy region, only a few nuclides are present and the statistical meaning of the distribution parameters becomes

TABLE II. Parameters obtained using a Gaussian fit for the system ^{37}Cl+^{40}Ca at 270 MeV. The energy loss ($E_{\rm loss}$) values have been corrected assuming equal division of the excitation energy.

$E_{\rm loss}$ (MeV)	$\langle Z\rangle$	$\langle N\rangle$	σ_Z^2	σ_N^2	ρ
8	17.12	19.67	0.237	0.289	0.073
	±0.05	±0.08	±0.021	±0.026	±0.065
12	16.97	19.60	0.345	0.596	0.152
	±0.05	±0.08	±0.023	±0.036	±0.043
16	16.96	19.26	0.617	0.921	0.375
	±0.05	±0.08	±0.025	±0.033	±0.025
20	16.91	19.02	0.919	1.142	0.559
	±0.05	±0.08	±0.029	±0.034	±0.016
24	16.84	18.89	1.104	1.388	0.660
	±0.05	±0.08	±0.034	±0.041	±0.014
28	16.79	18.71	1.310	1.859	0.725
	±0.05	±0.08	±0.040	±0.053	±0.011
32	16.69	18.51	1.713	2.404	0.799
	±0.05	±0.08	±0.047	±0.063	±0.008
36	16.57	18.26	2.142	3.079	0.860
	±0.05	±0.08	±0.055	±0.075	±0.006
40	16.47	18.14	2.635	3.630	0.883
	±0.05	±0.08	±0.047	±0.063	±0.004
44	16.42	18.00	3.296	4.460	0.906
	±0.06	±0.08	±0.079	±0.105	±0.004
48	16.31	17.82	3.812	5.250	0.921
	±0.06	±0.08	±0.078	±0.105	±0.003
52	16.22	17.69	4.737	6.401	0.934
	±0.06	±0.08	±0.092	±0.122	±0.002
56	16.12	17.56	5.776	7.842	0.948
	±0.06	±0.08	±0.109	±0.146	±0.002
60	15.94	17.35	6.801	9.102	0.955
	±0.06	±0.07	±0.092	±0.122	±0.001
64	15.84	17.23	8.231	10.959	0.964
	±0.06	±0.08	±0.170	±0.225	±0.001
68	15.65	17.02	9.849	13.087	0.969
	±0.07	±0.09	±0.211	±0.279	±0.001
72	15.48	16.83	11.955	15.921	0.974
	±0.07	±0.09	±0.274	±0.364	±0.001
76	15.25	16.60	13.875	18.819	0.976
	±0.07	±0.10	±0.350	±0.474	±0.001
80	14.98	16.29	16.607	22.320	0.981
	±0.09	±0.11	±0.493	±0.662	±0.001
84	14.83	16.12	18.366	25.187	0.982
	±0.09	±0.12	±0.586	±0.804	±0.001
88	14.66	15.94	20.409	27.848	0.985
	±0.10	±0.13	±0.721	±0.986	±0.001
92	14.71	15.98	21.889	30.254	0.985
	±0.11	±0.14	±0.881	±1.129	±0.001
96	14.78	16.08	21.385	29.989	0.986
	±0.10	±0.12	±0.664	±0.932	±0.001
100	15.15	16.54	16.850	24.016	0.982
	±0.11	±0.13	±0.709	±1.011	±0.001

questionable. Also, the results corresponding to ^{37}Cl on ^{40}Ca show significant differences at energy losses greater than about 80 MeV. These differences could be due to a non-Gaussian behavior of the distributions at those $E_{\rm loss}$ values. It would then appear that a moment analysis would be more appropriate for that energy region. However, it has to be kept in mind that a moment analysis is much more sensitive to data that has been cut off than a Gaussian fit and that these cutoffs, either purposely generated to exclude a nonphysical background or due to the dynamical range of the detector system, are always present.

The experimental distribution parameters presented in this paper correspond to the results from the two-dimensional Gaussian fit procedure, as presented in Refs. [5,8,9,24]. The errors that are quoted correspond only to

TABLE III. Parameters obtained using a Gaussian fit for the system ^{37}Cl+^{209}Bi at 270 MeV. The energy loss ($E_{\rm loss}$) values have been corrected assuming equal division of the excitation energy.

$E_{\rm loss}$ (MeV)	$\langle Z\rangle$	$\langle N\rangle$	σ_Z^2	σ_N^2	ρ
8	16.79	20.35	0.219	0.809	0.065
	±0.06	±0.11	±0.021	±0.079	±0.073
12	16.54	20.25	0.448	0.510	−0.181
	±0.05	±0.07	±0.080	±0.158	±0.191
16	16.51	20.30	0.367	0.580	0.397
	±0.06	±0.08	±0.022	±0.033	±0.036
20	16.42	20.22	0.501	1.018	0.410
	±0.05	±0.08	±0.017	±0.030	±0.020
24	16.16	20.06	0.697	1.197	0.416
	±0.06	±0.09	±0.034	±0.050	±0.028
28	16.02	19.91	0.773	1.356	0.462
	±0.06	±0.09	±0.039	±0.059	±0.027
32	15.92	19.78	0.783	1.488	0.438
	±0.06	±0.09	±0.040	±0.064	±0.028
36	15.90	19.68	0.838	1.678	0.490
	±0.06	±0.09	±0.040	±0.070	±0.025
40	15.81	19.53	0.903	1.774	0.563
	±0.06	±0.09	±0.044	±0.075	±0.024
44	15.65	19.41	0.953	1.863	0.594
	±0.06	±0.09	±0.048	±0.081	±0.024
48	15.55	19.34	1.033	1.946	0.554
	±0.06	±0.09	±0.049	±0.080	±0.024
52	15.45	19.18	1.080	2.109	0.618
	±0.06	±0.10	±0.054	±0.093	±0.023
56	15.34	19.00	1.167	2.329	0.627
	±0.06	±0.10	±0.058	±0.102	±0.022
60	15.15	18.91	1.304	2.753	0.670
	±0.07	±0.10	±0.067	±0.120	±0.021
64	14.96	18.58	1.297	2.607	0.686
	±0.07	±0.10	±0.068	±0.123	±0.021
68	15.02	18.57	1.615	2.971	0.746
	±0.07	±0.11	±0.085	±0.141	±0.018
72	14.78	18.26	1.498	2.972	0.743
	±0.070	±0.11	±0.085	±0.155	±0.019
76	14.67	18.16	1.572	3.276	0.771
	±0.073	±0.11	±0.099	±0.183	±0.020
80	14.68	17.99	2.325	4.645	0.838
	±0.09	±0.14	±0.140	±0.261	±0.015
84	14.48	17.97	2.401	4.609	0.836
	±0.09	±0.15	±0.149	±0.263	±0.016
88	14.12	17.67	2.413	4.954	0.843
	±0.09	±0.16	±0.169	±0.327	±0.016
92	13.73	17.05	2.096	3.640	0.762
	±0.09	±0.14	±0.161	±0.255	±0.026
96	13.79	17.20	2.303	5.253	0.866
	±0.10	±0.17	±0.188	±0.399	±0.017
100	13.17	16.42	1.425	2.343	0.823
	±0.09	±0.15	±0.151	±0.237	±0.028

those of the fitting procedure and do not reflect other possible sources. The statistical errors of the data are not considered explicitly in the fit procedure. However, the uncertainty in the fit results, calculated via chi squared, increases with the random fluctuations of the data points. In all the figures, error bars are indicated only if they are larger than the symbols. The resulting Gaussian parameters are summarized in Tables II–VI.

III. PRODUCT DISTRIBUTIONS

In this section, the secondary distributions of projectilelike fragments are presented in terms of their characteristic parameters as a function of energy loss, as derived from the two-dimensional Gaussian fit procedure. These parameters are $\langle Z \rangle$, $\langle N \rangle$, $\langle N \rangle / \langle Z \rangle$, the variances in charge and neutron number (σ_Z^2 , σ_N^2), and the cor-

TABLE IV. Parameters obtained using a Gaussian fit for the system ^{37}Cl+^{209}Bi at 270 MeV. The energy loss (E_{loss}) values have been corrected assuming thermal division of the excitation energy.

E_{loss} (MeV)	$\langle Z \rangle$	$\langle N \rangle$	σ_Z^2	σ_N^2	ρ
8	16.79	20.35	0.193	0.716	0.041
	±0.05	±0.08	±0.009	±0.031	±0.036
12	16.55	20.41	0.233	0.408	0.397
	±0.05	±0.08	±0.010	±0.018	±0.026
16	16.51	20.35	0.331	0.542	0.425
	±0.05	±0.08	±0.013	±0.019	±0.022
20	16.44	20.21	0.469	0.846	0.335
	±0.06	±0.09	±0.025	±0.041	±0.033
24	16.23	20.16	0.687	1.119	0.455
	±0.06	±0.09	±0.033	±0.047	±0.027
28	16.11	20.02	0.741	1.231	0.467
	±0.06	±0.09	±0.035	±0.050	±0.026
32	16.04	19.90	0.781	1.430	0.503
	±0.05	±0.08	±0.027	±0.044	±0.019
36	16.96	19.75	0.813	1.487	0.474
	±0.06	±0.09	±0.042	±0.066	±0.028
40	15.88	19.74	0.894	1.653	0.520
	±0.06	±0.09	±0.041	±0.067	±0.024
44	15.80	19.57	0.924	1.822	0.601
	±0.06	±0.09	±0.043	±0.074	±0.022
48	15.75	19.46	1.043	1.914	0.582
	±0.06	±0.09	±0.050	±0.082	±0.023
52	15.63	19.31	1.038	1.902	0.588
	±0.06	±0.09	±0.049	±0.080	±0.023
56	15.55	19.25	1.156	2.292	0.641
	±0.06	±0.09	±0.051	±0.087	±0.019
60	15.42	19.01	1.164	2.361	0.658
	±0.06	±0.10	±0.058	±0.103	±0.021
64	15.39	19.04	1.390	2.690	0.684
	±0.06	±0.10	±0.065	±0.113	±0.019
68	15.28	18.79	1.632	3.082	0.751
	±0.07	±0.11	±0.082	±0.140	±0.017
72	15.07	18.58	1.656	2.740	0.698
	±0.07	±0.11	±0.090	±0.134	±0.021
76	14.96	18.50	1.626	3.116	0.769
	±0.07	±0.11	±0.088	±0.153	±0.018
80	14.87	18.42	1.852	3.689	0.792
	±0.08	±0.12	±0.105	±0.196	±0.017
84	14.79	18.19	1.871	3.262	0.788
	±0.08	±0.12	±0.112	±0.179	±0.020
88	14.60	18.05	2.249	4.369	0.829
	±0.08	±0.13	±0.142	±0.258	±0.017
92	14.57	18.09	2.934	5.402	0.863
	±0.10	±0.16	±0.187	±0.321	±0.014
96	14.33	17.57	2.427	4.350	0.830
	±0.10	±0.14	±0.169	±0.290	±0.019
100	14.00	17.11	2.186	4.297	0.824
	±0.10	±0.16	±0.176	±0.310	±0.021

TABLE V. Parameters obtained using a Gaussian fit for the system ^{35}Cl+^{209}Bi at 528 MeV. The energy loss ($E_{\rm loss}$) values have been corrected assuming equal division of the excitation energy.

$E_{\rm loss}$ (MeV)	$\langle Z\rangle$	$\langle N\rangle$	σ_Z^2	σ_N^2	ρ
10	16.52	18.51	1.080	4.602	−0.356
	±0.06	±0.09	±0.033	±0.125	±0.018
20	16.23	18.40	1.193	5.366	−0.269
	±0.05	±0.08	±0.019	±0.074	±0.010
30	16.07	18.16	1.310	5.672	−0.283
	±0.05	±0.08	±0.017	±0.062	±0.008
40	15.80	18.14	1.489	6.491	−0.298
	±0.05	±0.08	±0.021	±0.073	±0.009
50	15.57	18.33	1.656	6.051	−0.251
	±0.05	±0.08	±0.024	±0.069	±0.009
60	15.43	18.44	1.785	4.980	−0.196
	±0.05	±0.08	±0.025	±0.060	±0.009
70	15.23	18.41	1.949	4.740	−0.156
	±0.06	±0.08	±0.041	±0.085	±0.014
80	14.81	18.79	2.279	5.099	−0.132
	±0.05	±0.07	±0.017	±0.029	±0.005
90	14.96	18.27	2.206	5.405	−0.005
	±0.06	±0.09	±0.056	±0.113	±0.017
100	14.73	18.25	2.084	4.951	0.133
	±0.06	±0.08	±0.040	±0.088	±0.012
110	14.28	18.69	2.286	5.956	0.249
	±0.06	±0.09	±0.058	±0.145	±0.016
130	14.29	17.90	2.351	7.174	0.352
	±0.06	±0.10	±0.067	±0.214	±0.017
150	13.76	16.77	1.996	7.290	0.307
	±0.06	±0.11	±0.062	±0.212	±0.020
170	13.11	16.17	1.732	5.515	0.242
	±0.06	±0.10	±0.053	±0.159	±0.020
190	12.62	14.75	1.683	4.923	0.204
	±0.07	±0.10	±0.061	±0.161	±0.024
210	11.76	13.64	1.616	4.757	0.195
	±0.07	±0.11	±0.078	±0.195	±0.031
230	11.28	11.70	1.641	4.351	0.250
	±0.08	±0.12	±0.090	±0.199	±0.036

relation coefficient (ρ). The evolution of the mass and charge centroids depends on the forces generated by the underlying dinuclear potential. In the case of symmetric systems and neglecting preequilibrium emission, no drift should occur in $\langle N\rangle$ or $\langle Z\rangle$ of the primary distributions. Therefore, the drifts in $\langle N\rangle$ and $\langle Z\rangle$ of the secondary distributions should be due solely to evaporative processes. On the other hand, for asymmetric systems gradients in the mass and isospin coordinates are expected to produce net drifts in $\langle N\rangle$ and $\langle Z\rangle$ of the primary distributions. The system ^{37}Cl on ^{40}Ca is nearly symmetric. The other two systems, ^{37}Cl on ^{209}Bi and ^{35}Cl on ^{209}Bi, have large asymmetries in the mass and isospin coordinates. A comparison between the last two systems should emphasize the effect of the N/Z ratio in the product distributions, since they have about the same mass asymmetry and different projectile N/Z value.

The variances are mostly sensitive to the type of mechanism involved in these reactions. For example, in the nucleon exchange mechanism the variance of the N-Z distribution is related to the number of nucleon exchanges between the reaction partners. The dependence between neutron and proton transfers is indicated by the correlation coefficient. A $\rho = 0$ (no correlation) means that the protons and neutrons are exchanged independently. Correlation is indicated by $\rho > 0$ and signifies that proton and neutron transfers occur preferentially in the same direction, for example, because of energetic constraints to the β-stability valley. A $\rho < 0$ (anticorrelation) would indicate that protons and neutrons are preferentially transferred in opposite directions.

Since the results presented here correspond to secondary distributions, it is important to keep in mind the effects of the sequential evaporation of neutrons and protons on the parameters of the distributions. Generally, the centroids of the secondary distributions show a negative shift with respect to those of the corresponding primary distributions. The magnitude of this shift will increase with excitation energy and, hence, energy loss. In heavy or neutron-rich systems, $\langle N\rangle$ should be mostly affected and $\langle Z\rangle$ may remain more or less unchanged. However, in light systems or at high energy losses, charge

TABLE VI. Parameters obtained using Gaussian fit for the system ^{35}Cl+^{209}Bi at 528 MeV. The energy loss (E_{loss}) values have been corrected assuming thermal division of the excitation energy.

E_{loss} (MeV)	$\langle Z \rangle$	$\langle N \rangle$	σ_Z^2	σ_N^2	ρ
10	16.54	18.48	1.046	4.472	−0.376
	±0.06	±0.10	±0.034	±0.133	±0.019
20	16.38	18.56	1.156	4.991	−0.290
	±0.05	±0.08	±0.021	±0.083	±0.011
30	16.01	18.47	1.244	5.064	−0.277
	±0.05	±0.08	±0.018	±0.064	±0.009
40	15.83	18.42	1.344	5.567	−0.285
	±0.05	±0.08	±0.018	±0.063	±0.008
50	15.67	18.22	1.511	6.173	−0.300
	±0.05	±0.08	±0.021	±0.070	±0.009
60	15.40	18.35	1.653	6.505	−0.287
	±0.05	±0.08	±0.024	±0.079	±0.010
70	15.56	18.39	1.755	6.020	−0.233
	±0.05	±0.08	±0.027	±0.074	±0.010
80	14.99	18.78	1.812	4.840	−0.197
	±0.06	±0.08	±0.037	±0.085	±0.014
90	14.95	18.64	1.972	4.722	−0.134
	±0.05	±0.08	±0.030	±0.063	±0.010
100	15.24	18.42	2.331	5.101	−0.132
	±0.06	±0.09	±0.061	±0.106	±0.017
110	15.14	18.30	2.345	5.450	−0.072
	±0.06	±0.08	±0.039	±0.071	±0.011
130	14.74	18.29	2.219	5.452	0.174
	±0.06	±0.09	±0.054	±0.127	±0.016
150	14.89	17.78	2.378	6.921	0.321
	±0.05	±0.07	±0.020	±0.063	±0.005
170	13.76	17.98	2.112	7.570	0.336
	±0.07	±0.10	±0.066	±0.238	±0.019
190	13.51	16.48	1.657	5.489	0.145
	±0.06	±0.10	±0.053	±0.165	±0.022
210	13.21	15.87	1.685	4.783	0.167
	±0.06	±0.10	±0.056	±0.150	±0.023
230	12.11	14.94	1.420	4.095	0.087
	±0.07	±0.10	±0.061	±0.144	±0.027

evaporation can become very significant. The variances are also affected by the evaporation process. Secondary distributions can be either narrower or wider than the primary ones. Also, sequential evaporation can significantly increase the coefficient of correlation as it focuses the distribution towards the β-stability line.

A. Centroids and neutron-to-proton ratios

The values of $\langle Z \rangle$, $\langle N \rangle$ and $\langle N \rangle / \langle Z \rangle$ as a function of energy loss are shown in Fig. 4 for the system ^{37}Cl on ^{40}Ca. The circles represent the experimental data. The $\langle Z \rangle$ and $\langle N \rangle$ decrease with increasing energy loss. The decrease in $\langle N \rangle$ is nearly a linear function. At 90 MeV of E_{loss}, $\langle N \rangle$ and $\langle Z \rangle$ have lost about 4.2 N units and 2.3 Z units, respectively. If the excitation energy is divided equally, the average amount of mass evaporated can be calculated [Eq. (1)] to be around 4 mass units, which is 2.5 mass units less than the experimental result. Therefore, it appears that the mass deficit in the projectilelike fragments cannot be accounted for by evaporation alone. Overall, it seems that there should be a net flow of nucleons from the projectile to the target to justify the mass deficit. The ratio $\langle N \rangle / \langle Z \rangle$ initially decreases, as would be expected from a process of charge equilibration, and after about 40 MeV of energy loss remains nearly constant at a value of about 1.09. This ratio is very close to the N/Z ratio of the composite system (1.08).

The results for $\langle Z \rangle$, $\langle N \rangle$, and $\langle N \rangle / \langle Z \rangle$ are shown in Fig. 5 for the system ^{37}Cl on ^{209}Bi. The circles and squares correspond to corrections of the energy-loss scale assuming equal and thermal division of the excitation energy, respectively. At low-energy loss, the differences between these corrections are not significant. However, after the first 20 MeV of energy loss, the $\langle Z \rangle$ and $\langle N \rangle$ corresponding to equal division of the excitation energy are increasingly smaller than those corresponding to thermal division. This result is expected because evaporation increases with excitation energy, and, at a given energy loss, the equal division of excitation energy will deposit more excitation in the lighter partner than does thermal division. The $\langle Z \rangle$ and $\langle N \rangle$ decrease with increasing en-

ergy loss. At 70 MeV of $E_{\rm loss}$, $\langle N\rangle$ and $\langle Z\rangle$ have lost about 1.6 N units and 1.0 Z units, respectively.

The $\langle N\rangle$ rises to a little over 20 for the first 20 MeV of $E_{\rm loss}$, while $\langle Z\rangle$ decreases steadily from 17. This seems to indicate a net transfer of neutrons from the target to the projectile and a net transfer of protons from the projectile to the target, for the lowest $E_{\rm loss}$. Both $\langle N\rangle$ and $\langle Z\rangle$ show an almost linear dependence over most of the $E_{\rm loss}$ range. The ratio $\langle N\rangle/\langle Z\rangle$ rises slightly, and reaches a constant value after about 20 MeV of energy loss. This value is around 1.24 and is far from the composite system value of 1.46.

Figure 6 shows the results for $\langle Z\rangle$, $\langle N\rangle$, and $\langle N\rangle/\langle Z\rangle$ as a function of $E_{\rm loss}$ for the system ^{35}Cl on ^{209}Bi. The circles and squares represent corrections of the energy-loss scale corresponding to equal and thermal division of the excitation energy, respectively. There are no significant differences between corrections for the first 100 MeV of $E_{\rm loss}$. After that the differences in $\langle Z\rangle$ start increasing with energy loss, reaching up to 2 Z units. The differences in $\langle N\rangle$ evolve similarly, giving differences of up to 4 N units. As expected, the $\langle Z\rangle$ and $\langle N\rangle$ corresponding to equal division of the excitation energy are smaller than those corresponding to thermal division. The value of $\langle Z\rangle$ decreases nearly monotonically with increasing energy loss. At 100 MeV of $E_{\rm loss}$ $\langle Z\rangle$ has lost about 2 Z units. The value of $\langle N\rangle$ remains approximately constant ($\approx$ 18.5) up to about 100 MeV of $E_{\rm loss}$; then it starts

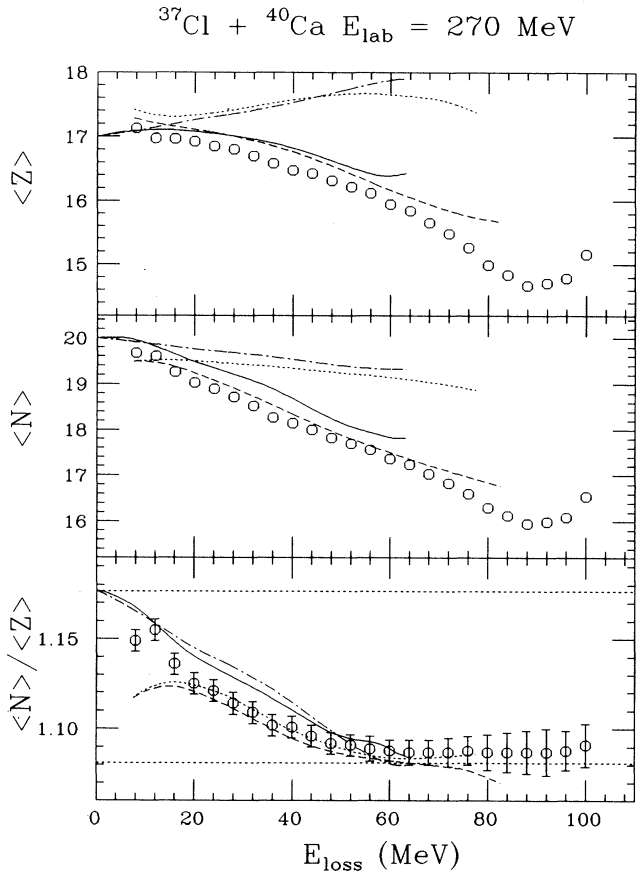

FIG. 4. Experimental results (circles) and model predictions for $\langle Z\rangle$, $\langle N\rangle$, and $\langle N\rangle/\langle Z\rangle$ corresponding to the secondary (post-evaporation) distributions of projectilelike fragments of the reaction ^{37}Cl + ^{40}Ca at 270 MeV as a function of energy loss. The dash-dotted lines and the dotted lines represent the result of the primary distributions predicted by Randrup's and Tassan-Got's models, respectively. The solid lines represent the results from Randrup's model and the dashed lines represent the results from Tassan-Got's model, after being corrected for evaporation using PACE II. The horizontal dotted lines represent the ratio N/Z of the projectile (top) and compound system (bottom), respectively.

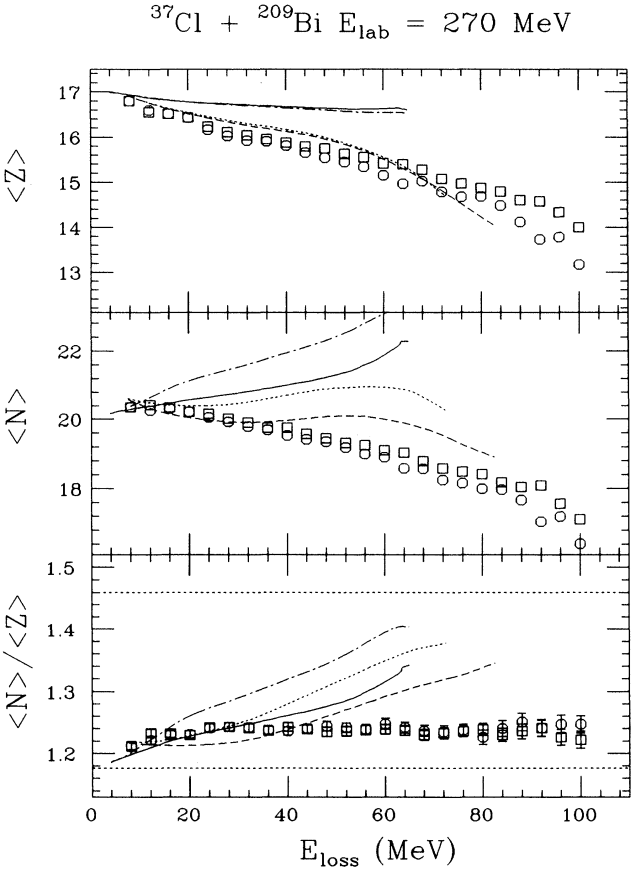

FIG. 5. Experimental results (circles and squares) and model predictions for $\langle Z\rangle$, $\langle N\rangle$, and $\langle N\rangle/\langle Z\rangle$ corresponding to the secondary distributions of projectilelike fragments of the reaction ^{37}Cl + ^{209}Bi at 270 MeV. The circles and squares represent the experimental results after correcting the energy-loss scale assuming equal and thermal division of the excitation energy, respectively. The dash-dotted lines and the dotted lines represent the result of the primary distributions predicted by Randrup's and Tassan-Got's models, respectively. The solid lines represent the results from Randrup's model and the dashed lines represent the results from Tassan-Got's model after being corrected for evaporation using PACE II. The horizontal dotted lines represent the ratio N/Z of the projectile (bottom) and compound system (top).

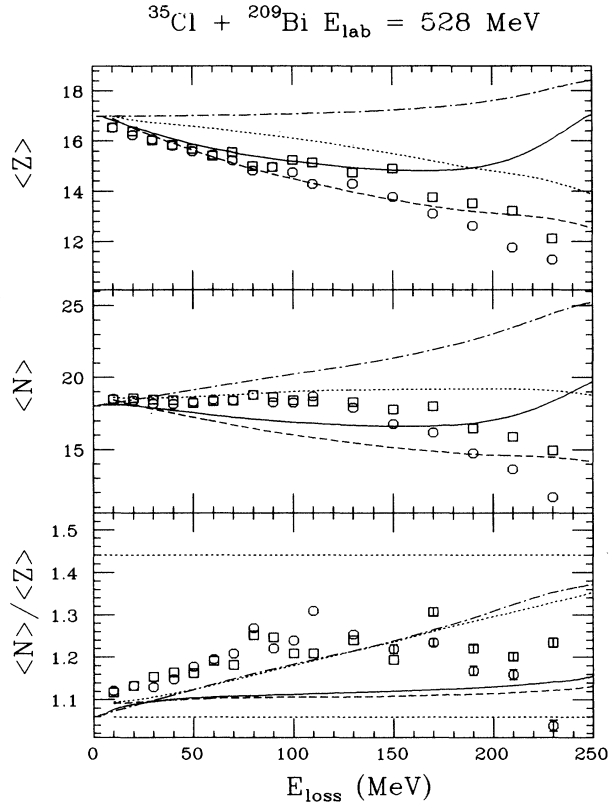

FIG. 6. Same as Fig. 5 for the reaction ^{35}Cl + ^{209}Bi at 528 MeV.

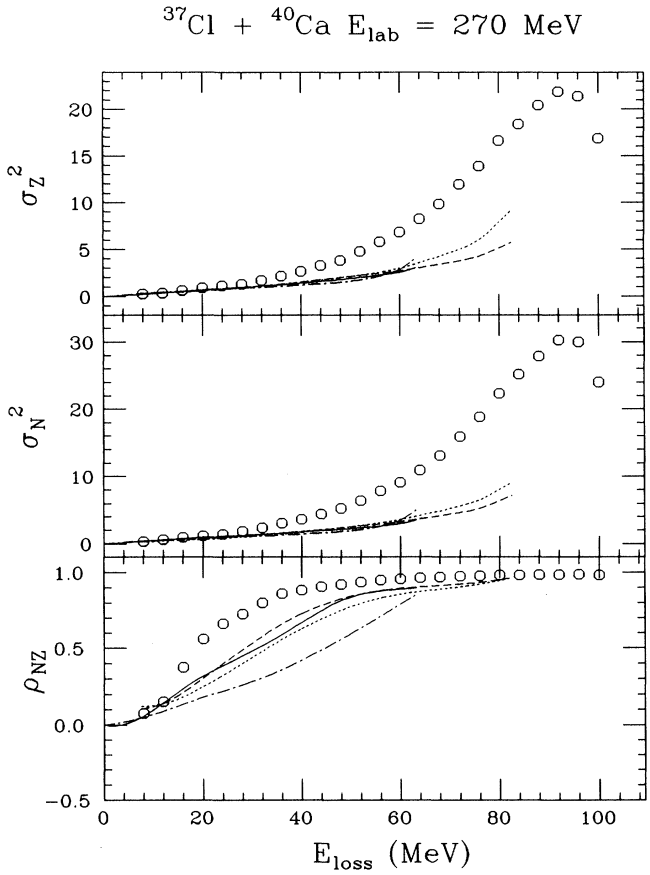

FIG. 7. Experimental results and model predictions for σ_Z^2, σ_N^2 , and ρ_{NZ} corresponding to the secondary distributions of projectilelike fragments of the reaction ^{37}Cl + ^{40}Ca at 270 MeV as a function of energy loss. Symbols are the same as in Fig. 4.

decreasing. For the first 100 MeV of $E_{\rm loss}$, the $\langle N\rangle/\langle Z\rangle$ ratio increases up to about 1.25. At $E_{\rm loss}$ larger than 100 MeV, the fluctuations make it difficult to establish a clear trend. However, the data points remain well below the N/Z ratio of the composite system. It must be pointed out that there could be a systematic error for the neutron numbers corresponding to Z <15, since the energy dependence of the mass centroids was established only up to Z=15. However, the direction of this error is not known and the $\langle N\rangle$ drift seems too large to be due only to this. As in the case of ^{37}Cl on ^{209}Bi, these results support a net flow of neutrons from the target to the projectile and of protons from the projectile to the target. However, the functional dependence of $\langle N\rangle$ shows a striking difference with respect to that case.

B. Variances and coefficients of correlation

In Fig. 7 the values of σ_Z^2, σ_N^2, and ρ are displayed as a function of energy loss for the system ^{37}Cl on ^{40}Ca. Both σ_Z^2 and σ_N^2 increase rapidly with $E_{\rm loss}$. At 90 MeV of $E_{\rm loss}$, the σ_Z^2 and σ_N^2 reach values of around 20 and 30, respectively. The correlation coefficient increases sharply with energy loss and between 40 and 60 MeV reaches a nearly constant value very close to 1.0. The rapid increase of the variances and the correlation coefficient with energy loss indicates that the product distributions readily group around a diagonal line in the N-Z plane.

The results of σ_Z^2, σ_N^2, and ρ are displayed as a function of energy loss for the system ^{37}Cl on ^{209}Bi at 7.3 MeV/nucleon in Fig. 8. As in the previous case, both σ_Z^2 and σ_N^2 increase with energy loss but, to a much lesser extent. At 70 MeV of $E_{\rm loss}$, the variances in N and Z are about 5 and 2.5, respectively. The correlation coefficient rises sharply to a value around 0.4 in the first 20 MeV of energy loss. After that, it follows a smooth linear rise reaching a value of 0.7 at 70 MeV of $E_{\rm loss}$.

For the system ^{35}Cl on ^{209}Bi at 15 MeV/nucleon, the results of σ_Z^2, σ_N^2, and ρ are shown in Fig. 9. Spurious contributions were observed in the mass coordinate around the elastic peak that could have affected the value of the variances. They should contribute only to the low-energy-loss portion of the spectra and affect mainly σ_N^2 and ρ, and to a lesser degree σ_Z^2. This could explain the hump observed in σ_N^2 at 50 MeV of $E_{\rm loss}$. However, after 50 MeV of $E_{\rm loss}$, the spectra are clean and it is possible to compare trends in the data with more confidence. The σ_Z^2 increases up to 100 MeV of energy loss, and from there on starts decreasing. The σ_N^2 seems to follow more or less the same behavior. This is an interesting feature that is not observed in the other two systems. In the

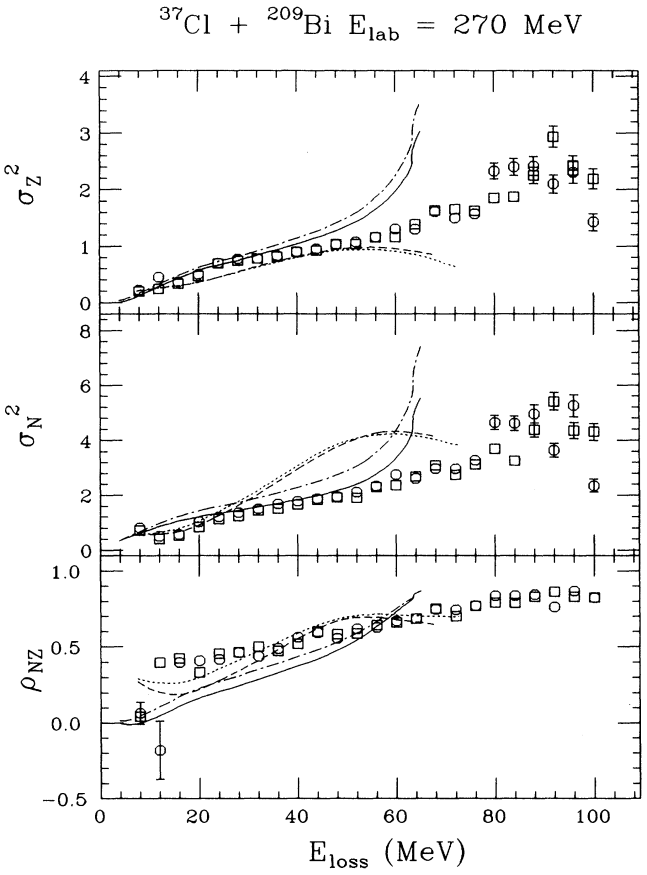

FIG. 8. Experimental results and model predictions for σ_Z^2, σ_N^2, and ρ_{NZ} corresponding to the secondary distributions of projectilelike fragments of the reaction ^{37}Cl + ^{209}Bi at 270 MeV as a function of energy loss. Symbols are the same as in Fig. 5.

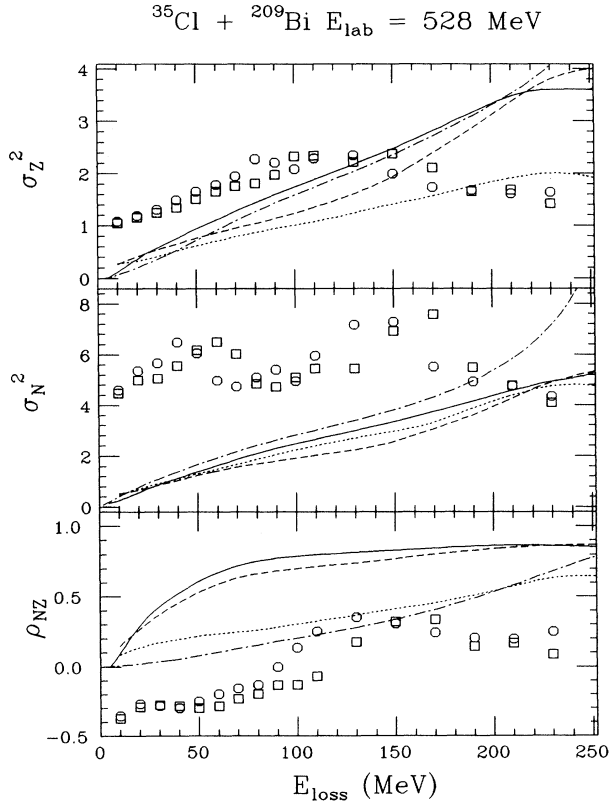

FIG. 9. Same as Fig. 8 for the reaction ^{35}Cl + ^{209}Bi at 528 MeV.

same energy region where the variances reach a maximum, there is a sudden change in the slope of the $\langle N \rangle$ and $\langle Z \rangle$ as a function of energy loss. The correlation coefficient shows a sudden increase at about 100 MeV of energy loss (going from negative to positive) and then remains approximately constant, but only at a value of < 0.5, much less than for other systems.

IV. COMPARISONS TO MODEL PREDICTIONS

The models used here are based on the nucleon exchange mechanism. In this scenario, it is assumed that nucleon exchange is the only important mechanism of dissipation. Therefore, the damping of the kinetic energy, the transport of angular momentum, and the evolution of the system in the N-Z plane are explained in terms of the exchange of nucleons between the reaction partners. The system is represented as two Fermi-Dirac gases that exchange particles. In Randrup's model [17] a mean trajectory approach is used. The dynamical equations for the mean trajectory are derived using the Lagrange-Rayleigh formulation of the equations of motion. The conservative driving forces are derived from the Lagrangian of the macroscopic system, the dissipative forces are obtained from the Rayleigh dissipation function, and the fluctuations of N and Z are predicted using a Fokker-Planck equation. Since the driving forces are derived using the Lagrangian, they implicitly contain kinetic terms (angular momentum, relative kinetic energy).

On the other hand, Tassan-Got's model [18] uses a Monte Carlo approach and operates in an event-by-event mode. An event starts with the projectile and target approaching in a Coulomb trajectory. When the two nuclei are within range of the nuclear field a window opens and stochastic transfers can occur. At this stage the relative motion and the dinuclear potential are solved numerically in steps. At each step the neutron and proton transfer probabilities are calculated. The possibility of occurrence of a transfer and the type of transfer is determined by random number generation for each step of the trajectory. If a transfer occurs, the characteristics of the nuclei are changed accordingly (mass, atomic number, angular momentum, excitation energy, etc.). The motion is conservative between transfers and only the transfers generate dissipation. The kinetic terms are not included in the determination of the net nucleon flux.

Model calculations for the three experimental systems were performed using the computer codes created by Randrup and Tassan-Got. Both codes predict primary distributions, which are given as a function of energy loss. To compare with experimental data, corrections for

evaporation were included using the evaporation code PACE II [20]. This evaporation code requires as input the excitation energy and the spin of the excited nucleus. In the case of Tassan-Got's code, the predicted primary distribution was discrete and every nucleus of the distribution had an associated excitation energy and spin that were subsequently used as inputs to the evaporation code. Randrup's code, on the other hand, predicted the primary distribution in terms of parameters of a two-dimensional Gaussian distribution in the N-Z plane, along with average values of spin and temperature. In this case every nuclide with an associated probability of over 5% in the N-Z plane was used as input to the evaporation code and the values of spin and temperature were assumed to be equal to the average values. The yields of the nuclei resulting from the evaporation simulation, properly normalized to the primary distribution, constitute the secondary distribution. A moment analysis was performed on these distributions to obtain their characteristic parameters as a function of energy loss. In the corresponding figures, model predictions corrected for evaporation are represented by a solid line in the case of Randrup's model and by a dashed line in the case of Tassan-Got's model. The primary distribution predictions are also included in some of the figures for reference. They correspond to the dash-dotted line in the case of Randrup's model and the dotted line in the case of Tassan-Got's model.

As seen in Fig. 4, there is a good agreement between the model predictions of $\langle Z\rangle$, $\langle N\rangle$, and their ratio and the data for the system ^{37}Cl on ^{40}Ca. However, Fig. 7 shows that, as the energy loss increases, the experimental variances become substantially larger than those predicted by both models. These larger variances are observed well above the entrance channel Coulomb barrier ($E_{\rm loss} \approx 93$ MeV). Therefore, it would appear that there are contributions to the width other than those generated in the current nucleon exchange scenario. The experimental correlation coefficient rises and tends to 1.0 faster than the model predictions.

For the system ^{37}Cl on ^{209}Bi, the experimental $\langle Z\rangle$ and $\langle N\rangle$ and their ratio are compared to model predictions in Fig. 5. Tassan-Got's model shows a good agreement in $\langle Z\rangle$ with the experimental data, while Randrup's model overestimates $\langle Z\rangle$. For the first 40 MeV of energy loss, Tassan-Got's prediction of $\langle N\rangle$ is also good, after that value of energy loss, it slightly overpredicts $\langle N\rangle$, but follows the trend of the experimental data.

Randrup's model predicts an increase of $\langle N\rangle$ with increasing energy loss, even after evaporation corrections, a behavior opposite to the trend of the experimental data. The N/Z values corresponding to the projectile and the composite system are represented in the figure by horizontal dashed lines. There do not seem to be significant differences in the ratio $\langle N\rangle/\langle Z\rangle$ between the models and experiment for the first 40 MeV of energy loss. At that point, the models predict an increase towards the composite system value of the $\langle N\rangle/\langle Z\rangle$ with energy loss, while the experimental values remain more or less constant at about 1.24.

The experimental variances and the correlation coefficient are compared to the models in Fig. 8. Randrup's model agrees very well with the experimental variances up to about 60 MeV of energy loss. Tassan-Got's model reproduces very well the Z variance, but it overestimates the N variance after the first 25 MeV of energy loss. The experimental correlation coefficient, as a function of energy loss, shows a sudden increase to a value of about 0.5, then a slow linear growth towards a value of 1.0. The models do not reproduce this behavior very well; they show an overall smooth increase of the coefficient with increasing energy loss.

In Fig. 6 the experimental values for $\langle Z\rangle$, $\langle N\rangle$, and the ratio $\langle N\rangle/\langle Z\rangle$ are compared to the model predictions for the system ^{35}Cl on ^{209}Bi. Tassan-Got's model gives a better overall agreement with the experimental $\langle Z\rangle$ than does Randrup's. However, both models fail to describe the evolution of the experimental $\langle N\rangle$ with energy loss and the ratio $\langle N\rangle/\langle Z\rangle$ is underestimated by both models. It is interesting to note that, while the experimental $\langle N\rangle/\langle Z\rangle$ increases towards the composite system value (1.44) for the first 100 MeV of energy loss, both models predict a nearly constant value around 1.10. This is in contrast with the predictions for the system ^{37}Cl on ^{209}Bi.

The comparison of model predictions to experimental variances and correlation coefficients for the system ^{35}Cl on ^{209}Bi can be found in Fig. 9. The experimental variances increase up to about 100 MeV of energy loss, where they reach a maximum and start to decrease slowly, while both models predict a steady increase of the variances with energy loss. This is an interesting feature that is not observed in the other two systems. In the same energy region where the variances reach a maximum, there is a sudden change in the slope of the average values of N and Z as a function of energy loss. These findings could indicate that a different type of mechanism is necessary at higher energy losses. A breakup of the projectilelike fragment is a possible explanation for these observations; it would explain both the narrowing of the variances and the sudden negative drifts in $\langle N\rangle$ and $\langle Z\rangle$. The experimental ρ is negative for the first 100 MeV of energy loss, in disagreement with both models, which predict a sudden rise followed by a smooth increase towards 1.0. However, it is not conclusive that there is anticorrelation, since the negative value could be the effect of the mass resolution.

For the asymmetric systems, it is instructive to look at the experimental averages for Z and N corresponding to different energy losses on the N-Z plane, as shown in Fig. 10 for the system ^{37}Cl on ^{209}Bi and in Fig. 11 for the system ^{35}Cl on ^{209}Bi. A line corresponding to the ratio N/Z of the composite system (dash-dotted line), and a β-stability line (dotted line) are included in the figures to serve as guides. The β-stability line was obtained using the mass equation from Ref. [26]. Both systems show a strong negative charge drift with production of neutron-rich projectilelike fragments. The evolution predicted by the models is also shown in both plots. It is clear that Randrup's model predictions (solid line) show significant departures from the experimental data in the N-Z plane. Tassan-Got's predictions (dashed line) follow more or less

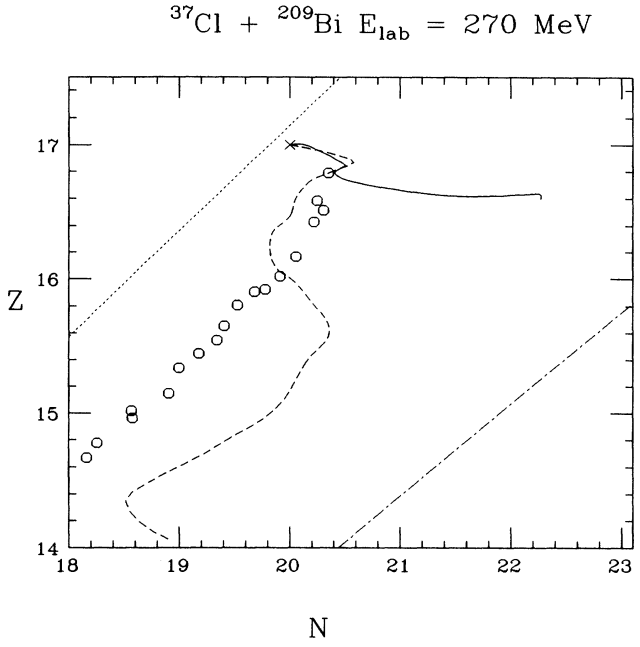

FIG. 10. Evolution of $\langle N \rangle$ and $\langle Z \rangle$ in the N-Z plane of the secondary projectilelike fragments of the reaction ^{37}Cl + ^{209}Bi at 270 MeV. The circles represent experimental values assuming equal excitation energy division, the solid and dashed lines represent Randrup and Tassan-Got's predictions, respectively. The dotted line corresponds to the valley of β stability and the dot-dashed line represents the ratio N/Z of the compound system.

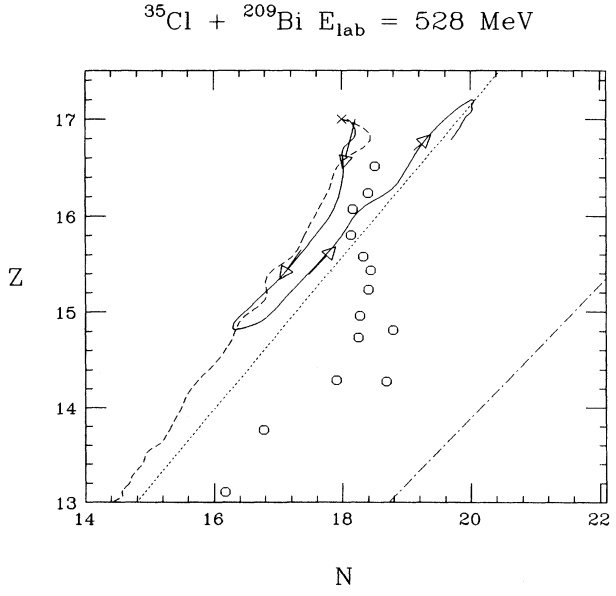

FIG. 11. Same as Fig. 10 for the reaction ^{35}Cl + ^{209}Bi at 528 MeV. The direction of the arrows indicate increasing energy loss for the solid line.

the trends of the data but fail to reproduce the details.

Using the nuclear exchange model, a linear expression can be derived [1] linking the variance in Z (or A) with the square root of the available relative kinetic energy ($T^{1/2}$) as defined by

$$T^{1/2} = (E_{\text{c.m.}} - E_{\text{loss}} - V_C)^{1/2}, \tag{3}$$

where $E_{\text{c.m.}}$ is the center-of-mass kinetic energy, and V_C is the Coulomb barrier. The theoretical linear dependence between $T^{1/2}$ and σ_Z^2 (Eq. (3.4.15) in Ref. [1]) is valid only at low-energy losses. However, this representation presents a different perspective and could help bring new insights in the interpretation of the data. The linear relation between $T^{1/2}$ and σ_Z^2 is valid for primary distributions, therefore, to test its validity with experimental data, the variances should be corrected for evaporation. However, Figs. 7, 8, and 9 indicate that there are not significant differences between the variances in Z and N between model calculated primary and secondary distributions.

For the three systems studied here, the square root of the available relative kinetic energy was plotted versus

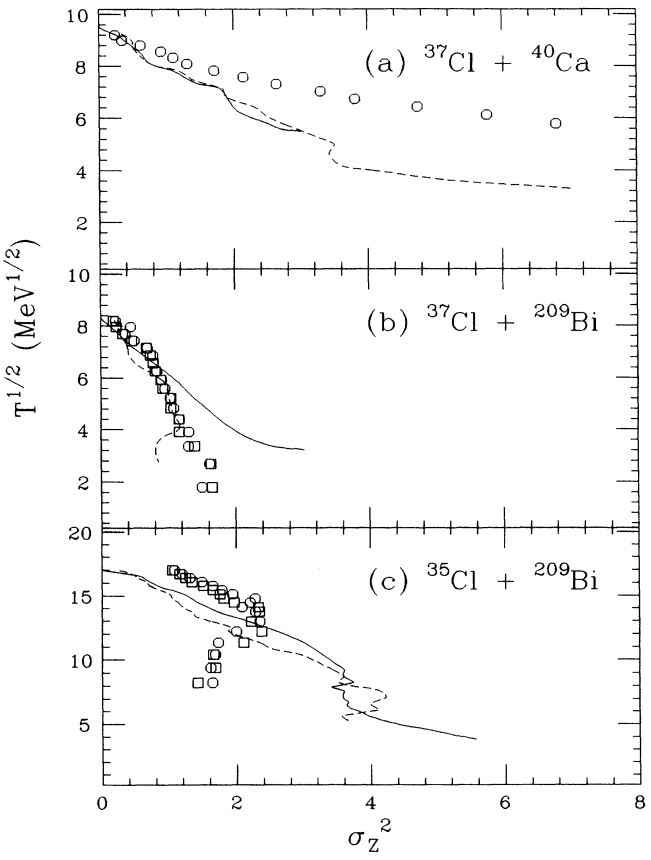

FIG. 12. Square root of the available relative kinetic energy ($T^{1/2}$) as a function of σ_Z^2 for the reactions: (a) ^{37}Cl + ^{40}Ca at 270 MeV, (b) ^{37}Cl + ^{209}Bi at 270 MeV, and (c) ^{35}Cl + ^{209}Bi at 528 MeV. Symbols are the same as in Figs. 4 and 5.

the Z variance of the secondary distributions for both the model calculations and the experimental results. For the system ^{37}Cl on ^{40}Ca, shown in Fig. 12(a), the experimental $T^{1/2}$ decreases with σ_Z^2 as expected, however, the models predict a much sharper decrease than that observed. If the variance is representative of the number of nucleon exchanges, then the case of ^{37}Cl on ^{40}Ca would suggest that the experimental exchanges are less effective at dissipating energy than the models predict.

In Fig. 12(b), $T^{1/2}$ is represented as a function of σ_Z^2 for the system ^{37}Cl on ^{209}Bi. The experimental data seem to fall between the two models but is in better overall agreement with Tassan-Got's model. There is a sharp change in the slope of the experimental data at a σ_Z^2 of about 0.8. Tassan-Got's model predictions approximately follow this slope; Randrup's predictions are linear up to a σ_Z^2 of about 2 and follow only the first points of the experimental data. The same plot for the system ^{35}Cl on ^{209}Bi can be found in Fig. 12(c). The experimental data show a linear dependence with σ_Z^2 up to a value of about 2.4 and then show a dramatic change from a negative to a positive slope. After that point, the value of σ_Z^2 changes very little, while $T^{1/2}$ continues decreasing. This behavior is inconsistent with a nucleon exchange mechanism, which predicts increasing variance with increasing energy loss. The slopes predicted by the models are in agreement with the experimental slope at low σ_Z^2. However, the $T^{1/2}$ values differ more or less by a constant.

V. COMPARISONS TO OTHER SYSTEMS

In making comparisons between different systems and bombarding energies it is important to remember that the deep-inelastic mechanism is a function of the relative velocity of the ions and, as a consequence, a function of the total kinetic energy and Coulomb barrier. Therefore, even at the same bombarding energy, the energy-loss range would not strictly scale between different systems. Thus, the comparisons between systems are made on a qualitative basis.

A negative drift in $\langle Z \rangle$ of the projectilelike fragments has been observed in many asymmetric systems in which the projectile has a lower N/Z ratio than the target [3–11]. This is evidence of a net flow of protons from the projectile to the target. Likewise, the increase in the N/Z ratio of the projectilelike fragments can be assigned to a net flow of neutrons from the target to the projectile. On the other hand, observations made on the system ^{136}Xe on ^{56}Fe at 5.9 MeV/nucleon, where the projectile has a higher ratio N/Z than the target, showed that the $\langle Z \rangle$ of the projectilelike fragments increased, while the $\langle N \rangle$ decreased [13]. Therefore, one can infer that the $\langle Z \rangle$ of the targetlike fragment decreased, while the $\langle N \rangle$ increased, in agreement with the other systems.

It is interesting to compare the results of ^{58}Ni (N/Z= 1.07) and ^{64}Ni (N/Z= 1.29) on ^{238}U (N/Z= 1.59) at 8.5 MeV/nucleon (see Fig. 5 in Ref. 8) to the results of the asymmetric systems studied here, ^{35}Cl (N/Z= 1.06) and ^{37}Cl (N/Z= 1.18) on ^{209}Bi (N/Z= 1.52), since they have similar N/Z ratios. The products of ^{37}Cl- and ^{64}Ni-induced reactions show a nearly linear and negative drift in $\langle Z \rangle$ and $\langle N \rangle$. On the other hand, the products of ^{35}Cl and ^{58}Ni show an almost constant value for $\langle N \rangle$ for the first 100 MeV of energy loss and a negative drift in $\langle Z \rangle$. This seems to indicate a strong correlation between the yields of products and the N/Z ratio. A mass asymmetry parameter can be defined as $(A_T - A_P)/(A_T + A_P)$, where A_T and A_P stand for the mass of the target and the projectile, respectively. For ^{58}Ni and ^{64}Ni on ^{238}U, and ^{35}Cl and ^{35}Cl on ^{209}Bi the values of this parameter are 0.61, 0.60, 0.71, and 0.70, respectively. Therefore, the previous observations show no correlation with the mass asymmetry parameter.

The experimental evidence seems to indicate that charge equilibrates faster than mass, and this could explain the evolution of asymmetric systems towards larger asymmetry. In principle, the mass and charge drifts could also be understood in terms of the PES gradient around the injection point. In this scenario, the mass and charge drifts would be expected to follow, more or less, the direction of the gradient in the N-Z plane. For a series of four projectiles on ^{238}U, de Souza *et al.* [14] have shown that the magnitude of the proton drifts correlate with the magnitude of the calculated PES gradients. Also, Planeta *et al.* [9] have shown that the mass and charge centroids of the system ^{58}Ni on ^{238}U closely follow the direction of the calculated gradient in the N-Z plane; however, the system ^{74}Ge on ^{165}Ho shows a much stronger negative charge drift than that expected from the gradient.

Any experimental observation is based on secondary distributions from which the characteristics of the primary distributions are inferred. It has generally been assumed that the evaporation process occurs mainly via neutron emission and has a negligible effect on Z. Therefore, it is implied that the $\langle Z \rangle$ of the secondary distribution is very close to that of the primary. But, it can be argued that charged-particle emission is an important evaporation process, especially for lighter systems. However, the production of neutron-rich projectile-like fragments, away from the β-stability line, seems to support the hypothesis on $\langle Z \rangle$. Since evaporation favors the formation of stable species, a neutron-rich secondary nucleus should originate via neutron emission from a primary nucleus with an even higher N/Z ratio.

Randrup's model predictions have been compared to the experimental distributions for several asymmetric system [7–9,11,12,15,16]. The model seems to always predict higher values for $\langle Z \rangle$ and $\langle N \rangle$ than the experimental ones. Tassan-Got's model is recent, and, hence, it has not been compared to as many systems as Randrup's. Comparisons performed to some of the published data showed good agreement between the experimental centroids and Tassan-Got's model predictions [19]. In the systems studied here, Tassan-Got's predictions reproduced the trends of the experimental centroids, but failed to account for the details of the functional dependence.

The variances are related to the number of nucleon exchanges in the statistical models, hence, they represent the nucleonic mobility and should not be very sensitive to the driving forces. For different systems at E= 8.5

MeV/nucleon of bombarding energy, the Z and N variances measured as a function of energy loss were found to be in fairly good quantitative agreement with each other [9,14]. The variances measured here for the system ^{37}Cl on ^{209}Bi at 7.3 MeV/nucleon also show good agreement with those of the systems at 8.5 MeV/nucleon. Since the systems compared have very different potential gradients on the N-Z plane, this finding supports the idea that the variances are mainly related to the nucleonic mobility, which should not differ too much among different systems. In general, it is observed that the variance in Z is smaller than the variance in N, roughly by a factor of 2.0. Randrup's model reproduced very well the experimental variances of several asymmetric systems [7–9,11,12,15,16]. It was also in good overall agreement with the variances observed here for the system ^{37}Cl on ^{209}Bi (E= 7.3 MeV/nucleon). Tassan-Got's model fairly reproduces the variances of the latter but exhibits a different functional dependence from Randrup's, especially at high-energy loss.

For the system ^{37}Cl on ^{40}Ca at 7.3 MeV/nucleon, the variances are much larger than those predicted by the models and those corresponding to the more asymmetric systems. The differences become larger with increasing energy loss and are large even at $E_{\rm loss}$ well before the value corresponding to the Coulomb barrier.

Particle evaporation cannot be responsible for the differences, since the evaporation applied to the theoretical distributions leaves the variances practically unaffected, as shown in Fig. 7. Similar observations have been made for the heavier symmetric system ^{56}Fe on ^{56}Fe at 8.3 MeV/nucleon.[5,15] This evidence may point to quite different dynamics for the nearly symmetric or symmetric systems as compared to the asymmetric ones. Under the light of the nucleon exchange model, the larger variances suggest more nucleon exchanges. This is compatible with the idea of the formation of a long-lived rotational dinuclear system with both nuclei exchanging nucleons. However, this would also imply that the nucleon exchanges do not dissipate energy as efficiently as in the asymmetric systems.

The correlation coefficient is a measure of the mutual dependence between neutron and proton transfers. The general trend in the evolution of the correlation coefficient as a function of energy loss is a sharp initial increase followed by a smooth growth towards 1.0. This indicates that the charge and mass exchanges become more correlated with increasing energy loss and increasing variance in N and Z. Some systems show negative correlation at low energy loss. However, it has been pointed out that at low-energy loss this could be explained as an effect of reaction Q values, and/or the small number of species present [5,8,9].

VI. SUMMARY

The deep-inelastic reactions corresponding to the systems ^{37}Cl on ^{40}Ca and ^{209}Bi at E= 7.3 MeV/nucleon, and ^{35}Cl on ^{209}Bi at E= 15 MeV/nucleon have been studied. The projectile-like fragments were completely characterized in terms of mass, charge, and energy. Mass and charge distributions were determined for all three systems as a function of energy loss in the N-Z plane. These distributions were characterized in terms of their centroids, variances, and coefficients of correlation.

For the almost symmetric system ^{37}Cl on ^{40}Ca the evolution of $\langle N\rangle$, $\langle Z\rangle$, and variances with energy loss seems consistent with a stochastic exchange of nucleons. The drift in the centroids can be explained by evaporative processes following the production of the primary fragments. The variances increase with energy loss, as would be expected from an increasing number of nucleon exchanges. However, as energy loss increases, the variances become much larger than those predicted from a nucleon exchange mechanism. This situation is very similar to that encountered in the symmetric system ^{56}Fe on ^{56}Fe (see Figs. 10 and 11 in Ref. [5]). The behavior of the ratio $\langle N\rangle/\langle Z\rangle$ is indicative of charge equilibration, reaching the value of the composite system (1.08) at about 60 MeV of energy loss. There is a strong correlation between N and Z, which shows that the exchange is constrained by Q-value considerations to the valley of β stability.

A very striking feature of the asymmetric systems studied here is the very low yield of products with Z higher than the projectile. The strong negative drift in $\langle Z\rangle$, accompanied by the formation of neutron-rich nuclei, indicates a net flow of charge towards the target and of neutrons towards the projectile. It is important to note that such a trend is an indication of the importance of the ratio N/Z of projectile and target in determining the underlying driving forces. A qualitative comparison of the evolution of $\langle N\rangle$ and $\langle Z\rangle$ with energy loss for the projectiles ^{37}Cl (N/Z= 1.18) and ^{35}Cl (N/Z= 1.06) gives additional support to this point. Both cases show a decrease in $\langle Z\rangle$ from the very initial values of energy loss. However, the ^{35}Cl products maintain a constant $\langle N\rangle$ over a wide range of energy losses, while the $\langle N\rangle$ of the ^{37}Cl products decrease. These observations agree with those of the systems ^{58}Ni and ^{64}Ni on ^{238}U at E= 8.5 MeV/nucleon [8] which, when compared to ^{35}Cl and ^{37}Cl on ^{209}Bi, have similar N/Z ratios, but different asymmetry parameters. It would appear that the N/Z ratios of the projectile and target play a major role in determining the product yields.

The evolution of the variances for the system ^{37}Cl on ^{209}Bi is in good agreement with other asymmetric systems, and with the predictions from a nucleon-exchange mechanism. Despite the mass resolution problems, the variances of the system ^{35}Cl on ^{209}Bi seem to indicate the same trend at low-energy losses. However, after the first 100 MeV of energy loss, the variances show a sudden decrease, contrary to what would be expected from a pure nucleon-exchange mechanism. The coefficient of correlation increases with energy loss for the system ^{37}Cl on ^{209}Bi, as expected from a correlated nucleon exchange process. In the ^{35}Cl on ^{209}Bi system it is difficult to interpret the negative value of this coefficient in the first 100 MeV of energy loss as anticorrelation, since this could be an experimental artifact due to the poor mass resolution. Negative coefficients of correlation have been reported at very-low-energy losses for other systems [5,8,9], but there, as here, anticorrelation was not conclusive.

Stochastic nucleon-exchange models have been relatively successful in reproducing some of the features of the deep-inelastic reactions. In the case of asymmetric systems, the good agreement generally found between the experimental and predicted variances supports the nucleon exchange mechanism for these reactions. However, the mass and charge drifts are not properly accounted for. In this type of mechanism, the variances are directly proportional to the sum of the (large) nucleon currents between the projectile and target, and the drifts are proportional to their difference [13]. As a consequence, the drifts are more sensitive to the details of the underlying potential. The two models used here reproduce the mass and charge drift of the almost symmetric system very well, but they both underestimate the variances at high-energy loss. Randrup's model overpredicts $\langle N \rangle$ and $\langle Z \rangle$ for the asymmetric systems, while Tassan-Got's model gives a better qualitative agreement with the data but still fails to account for the details. The variances of the asymmetric systems are in overall agreement with the predictions of both models.

It is interesting that two models that are very similar in their physical foundations predict such different trends for the mass and charge drift of asymmetric systems. According to Tassan-Got, the main difference between the two models is Randrup's use of the Lagrangian to derive the driving forces; the inclusion of kinetic terms in the potential (in particular rotational energy) that are not present in Tassan-Got's description accounts for the discrepancy. Pal and Chattopadhay [27] concluded that the inclusion of trajectory fluctuations in their calculations resulted in a much better agreement with the experiment than the use of the mean trajectory method (Randrup's model). It has also been suggested that the consideration of non-Markovian effects can also give a better description of the experimental data [28]. Overall, this stresses the need for a more realistic and quantitative description of the driving forces acting on the dinuclear system.

It is apparent that, while there is a basic understanding of the deep-inelastic process, there is still a need for more detailed experiments to be able to reconstruct these reactions with a minimum of assumptions. In general, coincidence measurements of projectilelike and targetlike fragments combined with the determination of evaporation products are necessary to provide new insights. Recent experiments suggest that deep-inelastic processes also occur at intermediate energies (of the order of the Fermi energy $E_F \approx 37$ MeV) [18,19,29]. Hopefully, this will provide a renewed interest in the study of the deep-inelastic mechanism.

ACKNOWLEDGMENTS

The authors would like to thank V.E. Viola, R.R. Betts, and B.G. Glagola for their help during the Argonne experiment, and L. Tassan-Got and J. Randrup for facilitating the computer codes. The useful discussions with L. Tassan-Got are also gratefully acknowledged. This work was supported by the U.S. Department of Energy under Grant No. DEFG05-87ER40321 and the National Science Foundation.

[1] W.U. Schröder and J.R. Huizenga, *Treatise on Heavy-Ion Science*, edited by D.A. Bromley (Plenum, New York, 1984), Vol. 2, p. 115.

[2] R.A. Broglia, C.H. Dasso, and A. Winther, Phys. Lett. **53B**, 301 (1974); **61B**, 113 (1976).

[3] D.R. Benton, H. Breuer, F. Khazaie, K. Kwiatkowski, V.E. Viola, S. Bradley, A.C. Mignerey, and A.P. Weston-Dawkes, Phys. Rev. C **38**, 1207 (1988); Phys. Lett. B **185**, 326 (1987).

[4] H. Breuer, B.G. Glagola, V.E. Viola, K.L. Wolf, A.C. Mignerey, J.R. Birkelund, D. Hilscher, A.D. Hoover, J.R. Huizenga, W.U. Schröder, and W.W. Wilcke, Phys. Rev. Lett. **43**, 191 (1979).

[5] H. Breuer, A.C. Mignerey, V.E. Viola, K.L. Wolf, J.R. Birkelund, D. Hilscher, J.R. Huizenga, W.U. Schröder, and W.W. Wilcke, Phys. Rev. C **28**, 1080 (1983).

[6] A.D. Hoover, J.R. Birkelund, D. Hilscher, W.U. Schröder, W.W. Wilcke, J.R. Huizenga, H. Breuer, A.C. Mignerey, V.E. Viola, and K.L. Wolf, Phys. Rev. C **25**, 256 (1982).

[7] V. Penumetcha, G.A. Petitt, T.C. Awes, J.R. Beene, R.L. Ferguson, F.E. Obenshain, F. Plasil, G.R. Young, and S.P. Sorensen, Phys. Rev. C **42**, 1489 (1990).

[8] R. Planeta, S.H. Zhou, K. Kwiatkowski, W.G. Wilson, V.E. Viola, H. Breuer, D. Benton, F. Khazaie, R.J. McDonald, A.C. Mignerey, A. Weston-Dawkes, R.T. de Souza, and W.U. Schröder, Phys. Rev. C **38**, 195 (1988).

[9] R. Planeta, K. Kwiatkowski, S.H. Zhou, V.E. Viola, H. Breuer, M.A. McMahan, W. Kehoe, and A.C. Mignerey, Phys. Rev. C **41**, 942 (1990).

[10] K. Sapotta, R. Bass, V. Hartmann, H. Noll, R.E. Renfordt, and K. Stelzer, Phys. Rev. C **31**, 1297 (1985).

[11] R.T. de Souza, J.R. Huizenga, and W.U. Schröder, Phys. Rev. C **37**, 1901 (1988).

[12] R.T. de Souza, W.U. Schröder, J.R. Huizenga, J. Toke, S.S. Datta, and J.L. Wile, Phys. Rev. C **39**, 114 (1989).

[13] D. Schüll, W.C. Shen, H. Freiesleben, R. Bock, F. Busch, D. Bangert, W. Pfeffer, and F. Pühlhofer, Phys. Lett. B **102**, 116 (1981).

[14] R.T. de Souza, W.U. Schröder, J.R. Huizenga, R. Planeta, K. Kwiatkowski, V.E. Viola, and H. Breuer, Phys. Rev. C **37**, 1783 (1988).

[15] D.K. Lock, R. Vandenbosch, and J. Randrup, Phys. Rev. C **31**, 1268 (1985).

[16] J.L. Wile, S.S. Datta, W.U. Schröder, J.R. Huizenga, R.T. de Souza, and D. Pade, Phys. Rev. C **40**, 1700 (1989).

[17] J. Randrup, *Nucl. Phys.* **A307**, 319 (1978); **A327**, 490 (1979); **A383**, 468 (1982).

[18] L. Tassan-Got, Ph.D. thesis INPO-T-89-02, University of Paris Sud, Orsay, France, 1988; L. Tassan-Got and C. Stéphan, Nucl. Phys. **A524**, 121 (1991).

[19] B. Borderie, M.F. Rivet, and L. Tassan-Got, Ann. Phys. (Paris) **15**, 287 (1990).

[20] A. Gavron, Phys. Rev. C **21**, 230 (1980).
[21] H. Breuer *et al.*, LISA Collaboration; Department of Physics and Astronomy, University of Maryland, 1989.
[22] J.B. Moulton, J.E. Stephenson, R.P. Schmitt, and G. Wozniak, Nucl. Instrum. Methods **157**, 325 (1978).
[23] A.A. Marchetti, Ph.D. thesis DOE/ER/40321-8, University of Maryland, College Park, 1991; A.A. Marchetti, and A.C. Mignerey, Nucl. Instrum. Methods A **324**, 288 (1993).
[24] H. Breuer, N.R. Yoder, A.C. Mignerey, V.E. Viola, K. Kwiatkowski, and K.L. Wolf, Nucl. Instrum. Methods **204**, 419 (1983).
[25] K. Kwiatkowski, R. Planeta, S.H. Zhou, V.E. Viola, H. Breuer, M.A. McMahan, and A.C. Mignerey, Phys. Rev. C **41**, 958 (1990).
[26] L. Valentin, *Nuclei and Particles* (North-Holland, New York, 1975), Vol. 1, p. 120.
[27] D. Pal and S. Chattopadhay, Phys. Rev. C **41**, 390 (1990).
[28] D. Pal, S. Chattopadhay, and K. Kar, J. Phys. G **14**, 1083 (1988).
[29] B. Borderie, M. Montoya, M.F. Rivet, D. Jouan, C. Cabot, H. Fuchs, D. Gardes, H. Gauvin, D. Jacquet, and F. Monnet, Phys. Lett. B **205**, 26 (1988).